INSTITUTE OF PHYSICS PUBLISHING NANOTECHNOLOGY
Nanotechnology **17** (2006) 3436–3441 doi:10.1088/0957-4484/17/14/015

Chemical identification of point defects and adsorbates on a metal oxide surface by atomic force microscopy

Jeppe V Lauritsen[1], Adam S Foster[2], Georg H Olesen[1], Mona C Christensen[1], Angelika Kühnle[3], Stig Helveg[4], Jens R Rostrup-Nielsen[4], Bjerne S Clausen[4], Michael Reichling[3] and Flemming Besenbacher[1,5]

[1] Interdisciplinary Nanoscience Center (iNANO) and Department of Physics and Astronomy, Aarhus University, 8000 Aarhus C, Denmark
[2] Laboratory of Physics, Helsinki University of Technology, PO Box 1100, 02015 HUT, Finland
[3] Fachbereich Physik, Universität Osnabrück, Barbarastrasse 7, 49076 Osnabrück, Germany
[4] Haldor Topsøe, A/S, Nymøllevej 55, 2800 Kongens, Lyngby, Denmark

Received 13 April 2006, in final form 25 May 2006
Published 20 June 2006
Online at stacks.iop.org/Nano/17/3436

Abstract
Atomic force microscopy in the non-contact mode (nc-AFM) can provide atom-resolved images of the surface of, in principle, any material independent of its conductivity. Due to the complex mechanisms involved in the contrast formation in nc-AFM imaging, it is, however, far from trivial to identify individual surface atoms or adsorbates from AFM images. In this work, we successfully demonstrate how to extract detailed information about defects and the chemical identity of adsorbates on a metal oxide surface from nc-AFM images. We make use of the observation that the apex of the AFM tip can be altered to expose either a positive or negative tip termination. The complementary set of images recorded with the two tip terminations unambiguously define the ionic sub-lattices and reveal the exact positions of oxygen vacancies and hydroxyl (OH) defects on a TiO_2 surface. Chemical specificity is extracted by comparing the characteristic contrast patterns of the defects with results from comprehensive AFM simulations. Our methodology of analysis is generally applicable and may be pivotal for uncovering surface defects and adsorbates on other transition metal oxides designed for heterogeneous catalysis, photo-electrolysis or biocompatibility.

Scanning probe microscopy has become the preferred technique for investigating the atomic-scale realm of surfaces. The scanning tunnelling microscope (STM), in particular, has provided unprecedented and extensive insight into the atomic-scale structure and the nature of adsorbates and point defects on a variety of electrically conducting surfaces [1–3]. The closely related atomic force microscope (AFM) has matured enormously since its introduction 20 years ago [4], and in contrast to STM, the AFM operated in the non-contact mode (nc-AFM) is capable of providing genuine, atomic-scale insight into the surface structure of in principle any material independent of its conductivity [5–7]. The interest to further develop AFM as an analysis tool to investigate the surface structure of the whole range of non-conducting materials is therefore immense, and recent experiments have shown that it is indeed possible to obtain atomically resolved AFM images on a number of clean insulator surfaces [8–10]. One of the inherent limitations of both STM and AFM is, however, the missing chemical specificity of the surface atoms and adsorbates observed in atom-resolved images. The contrast in atom-resolved STM images often reflects a rather complicated convolution of electronic and geometric structure [11]. This is especially true for materials with an electronic band gap like TiO_2, and until now, no satisfactory identification of the defect in this surface based on a direct and unambiguous interpretation of their appearance in STM [12] or AFM [6] has

[5] Author to whom any correspondence should be addressed.

been given. Instead chemical identification was very recently performed indirectly by matching the dynamic behaviour of defects observed with time-resolved STM with their estimated diffusion rates and relative adsorption energies from density functional calculations [13] or on the basis of cycles of reacting the surface with water vapour and subsequently removing adsorbates by field-induced desorption with the STM tip [14]. For the AFM, it is possible to interpret experiments and extract detailed information about the chemical specificity of individual surface atoms or adsorbates by modelling the complex mechanisms involved in the atomic-scale contrast formation [15, 16]. In this paper, we demonstrate the identification of single oxygen vacancy defects, and two different hydroxyl species on a $TiO_2(110)$ metal oxide surface in a direct way by combination of AFM experiments.

1. Methods

1.1. Experimental details

Experiments were performed at room temperature in an ultra-high vacuum chamber with a base pressure better than 1.0×10^{-10} mbar equipped with standard surface preparation techniques and a commercial beam-deflection AFM (Omicron VT-AFM/STM). A polished rutile $TiO_2(110)$ single crystal was prepared by several cycles of Ar^+ ion bombardment and annealing to 620 °C. Images were recorded in the non-contact AFM mode of operation, where the frequency shift of an oscillating cantilever induced by the interaction of a tip mounted at the end of the cantilever with the surface is measured and the tip movement is controlled to follow the contours of constant frequency shift Δf. To improve imaging results, FM demodulation was performed with an easyPLL unit (Nanosurf). We used unconditioned tips (n-doped Si, Nanosensors, type NCH), and typically contacted the surface with the tip several times before obtaining good resolution. The cantilever was excited to vibration at its resonance frequency of approximately 308 kHz with its amplitude stabilized to about 30 nm. To compensate electrostatic forces due to differences in work function and surface charging, we carefully adjusted the bias voltage V_{cp} on the tip relative to the sample to the point where long-range electrostatic forces were minimized for each experiment.

1.2. Theory

The rutile $TiO_2(110)$ surface was represented by a $(6 \times 3 \times 3)$ unit cell, which was deep enough to converge the surface structure, and large enough to avoid spurious interactions between adsorbates. The calculation of the tip–surface interactions on the microscopic scale were performed using static atomistic simulations, 2D-periodic codes [17] and GULP [18]. This simulation technique uses point charges and polarizable shells to represent atoms, and pair potentials to represent atomic interactions. The pair potential parameters for the TiO_2 surface and its interaction with water were taken from [19], and have been extensively tested against both first principles calculations and experimental data. The remaining parameters for the tip and tip–surface interaction were taken from [20]. The vacancy was represented by first removing a bridging oxygen, and then changing the balance of charge within the vacancy and on the neighbouring 5- and 6-coordinated Ti atoms. We thus considered several models of the oxygen vacancy in TiO_2, from models based on hybrid-DFT calculations, which predict full localization of the electrons on neighbouring Ti atoms [21], to standard DFT methods, predicting significant electron density remaining in the vacancy [22]. Only in the latter case could we find agreement with the experimental interaction strength.

To identify the surface defects on TiO_2 in the experimental observations, we performed atomistic AFM simulations parameterized on density functional theory (DFT) calculations of the $TiO_2(110)$ surface using a metal oxide cluster tip model, namely an MgO cube terminating the tip. Such a cluster model provides a well-defined nanoprobe where the cube can be oriented to expose either a positive (Mg^{2+}) or negative (O^{2-}) electrostatic potential from the tip apex [23–25]. We also considered several other tip models in the simulations in order to test the influence of hydrogen or hydroxyl adsorbates on the tip, including Si, SiOH, SiO_2, TiO_2, and MgOH tips. These other tip models are all plausible, but did not reproduce well the experimental results presented here, and the modelling for these alternative tip choices will be discussed elsewhere. Our conclusion is that the MgO tip represents a reasonable general model of an ionic tip due to the dominance of electrostatics in the imaging interactions. In order to generate images which can be compared to experiment, it is important to include the long-range macroscopic van der Waals interaction between tip and surface [23]. This force is mainly determined by the radius of the tip and the Hamaker constant of the tip–surface system. Since the tip is likely originally oxidized silicon, we fix the Hamaker constant to the value for SiO_2–TiO_2 [26] and fit the radius to reproduce the experimentally measured contrast (defined as the corrugation of the Ti relative to the O rows) at the set-point for the constant frequency change. Microscopic and macroscopic forces are combined to provide a total map of the force across the surface. This is then used in a simple model [23] of the cantilever oscillations using experimental parameters to provide a simulated image for a given constant frequency change at the experimentally measured contrast. For comparison, the simulated images were produced at contrasts of 61 pm (picometre) for the negative tip and 60 pm for the positive tip, compared to 58 ± 10 pm and 70 ± 10 pm for the equivalent experimental results.

2. Results and discussion

When an AFM is operated in the non-contact mode, the contrast is generated by the detection of small variations in the tip–surface force acting on an oscillating tip scanning the surface at a sub-nanometre distance [27, 28]. Tip–surface forces include both long-range van der Waals forces and short-range chemical forces emanating from the outermost tip apex, with the latter being responsible for atomic-scale contrast formation. Our main finding for the present investigation of the $TiO_2(110)$ surface is concerned with the observation of two significantly different types of contrast pattern in highly resolved AFM images recorded at room temperature as shown in figures 1(a) and (b), respectively. The characteristic row structure associated with the $TiO_2(110)$ (1×1) surface (see figure 1(d)) is clearly visible as a dark–bright stripe pattern, associated with rows of two-fold coordinated protruding O^{2-} ions or rows of five-fold coordinated Ti^{4+} ions. Additionally, both images show a small population of point-like defects.

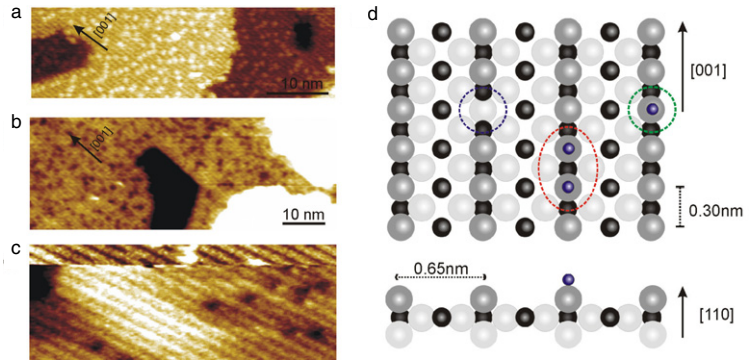

Figure 1. Two large-scale nc-AFM images of $TiO_2(110)$ recorded at room temperature. The images show the two predominant contrast patterns obtained after contacting the tip gently with the surface. Parameters: (a) 50 nm × 15 nm, $\Delta f = -14.5$ Hz and (b) 70 nm × 25 nm, $\Delta f = -14.3$ Hz. (c) Example of a change of the tip apex from a positive to a negative termination induced by scanning over a step edge on the $TiO_2(110)$ surface. In order not to induce a further change in resolution, the tip was in this case moved from the step edge after the change in contrast. (d) Ball model of rutile $TiO_2(110)$ (1 × 1). The surface exposes rows of bridging O^{2-} atoms protruding above a plane of oxygen atoms, and rows of five-coordinated Ti^{4+} atoms located geometrically lower. Large (light grey) and smaller (black) atom balls symbolize oxygen and titanium, respectively. Hydrogen atoms in the OH groups are represented by smaller dark blue balls. Also shown in the ball model are the three predominant types of defect present on $TiO_2(110)$ in the initial hours after a UHV preparation: an oxygen vacancy (i.e. a missing two-fold coordinated O atom), double OH formed by water dissociation in the vacancy, and single OH groups, respectively.

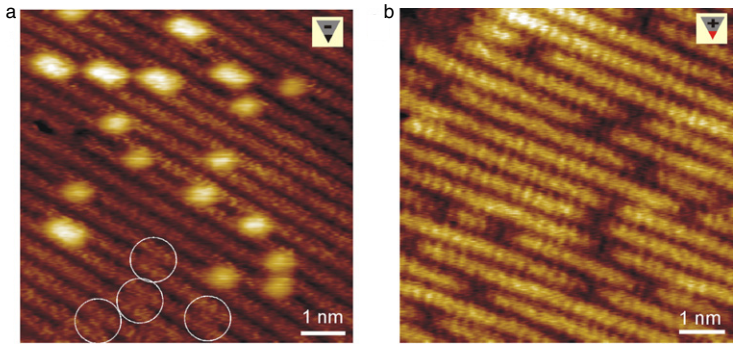

Figure 2. High-resolution nc-AFM images of the $TiO_2(110)$ surface obtained with a negatively and positively terminated tip, respectively. The polarity of the tip is indicated by the triangular symbols. Image parameters: (a) size is 10 nm × 10 nm, $\Delta f = -14.4$ Hz and $V_{cp} = +1.54$ V; (b) size is 7.3 nm × 9.3 nm, $\Delta f = -36.1$ Hz and $V_{cp} = +1.70$ V.

Both the coverage and the distribution of these defects are measured to be similar (around 3% of a monolayer), but whereas figure 1(a) reveals bright protrusions, the contrast is inverted in figure 1(b) and point-like depressions with a similar size are clearly observed. During the experiments, we occasionally observed that it is possible to change back and forth between the two predominant types of imaging contrast without a significant deterioration of the resolution. The tip change could be provoked by scanning the AFM tip at a close distance to the surface near a TiO_2 step edge until a change in the contrast was observed. A clear example is shown in figure 1(c), where the lower part corresponds to the contrast observed in figure 1(b) (holes). The slow scan direction is from bottom to top and the contrast is observed to shift to the mode also observed in figure 1(a) (protrusions) when the tip reaches the step edge visible in the upper right corner. The induced tip changes are thus considered to be a result of a multiple-atom exchange between the surface and tip, thus forming a nanotip sharp enough to provide atomic resolution. We never observed both types of contrast associated with the defects coexisting in the same image without a clear change of the tip termination and, therefore, we conclude that the *same types* of point-like surface defects are imaged under the conditions of our experiment, and that the difference in AFM imaging contrast of the defects in figures 1(a) and (b) is caused by a change in the short-range tip–surface interaction induced by the change of the tip apex termination.

Figures 2(a) and (b) show atom-resolved AFM images of the TiO_2 surface obtained with the two different types of tip termination. Again the row structure is apparent, but for one tip termination, a number of protrusions are clearly positioned in between the bright rows (figure 2(a)), whereas for the other tip termination defects are imaged as dark pits located exactly in registry with the bright rows (figure 2(b)). The observed contrast reversal together with the observation of the point-like defects allows for an unambiguous identification of the atomic species imaged. Our interpretation is based on the finding that AFM contrast at the atomic scale on surfaces exposing different atomic species (e.g. O^{2-} or Ti^{4+}) is often not simply determined by surface topography, but rather that the particular sub-lattice imaged with bright contrast is determined by the polarity of the apex terminating the AFM tip [29, 30]. In our experiments, the silicon AFM tip is terminated by a cluster of a polar material, presumably SiO_2 or TiO_2 picked up from the surface, that functionalizes the tip in one of two complementary states: an *anion* at

the tip apex yields a bright contrast (corresponding to a strong attraction) for the positively charged titanium sub-lattice (formally Ti^{4+}), while imaging with a *cation* at the tip apex oppositely yields a bright contrast for the negatively charged oxygen rows (formally O^{2-}). $TiO_2(110)$ is one of the most intensively studied metal oxide surfaces, and previous work has revealed that a well-prepared $TiO_2(110)$ (1×1) surface under ultra-high vacuum contains a low concentration of oxygen vacancy defects associated with missing atoms in the bridging O^{2-} rows [31]. Furthermore, it has been shown that the oxygen vacancies are very reactive [32–34], and at very low pressure conditions even trace amounts of water from the residual gas dissociate at the oxygen vacancies leading to the formation of hydroxyl (OH) groups on the oxygen rows (see figure 1(d)) [12, 13, 31, 35]. Initially, hydroxyls may appear as pairs of OH (so-called double hydroxyls), but on a timescale of hours the double OH will separate into single OH groups on a surface kept at room temperature [13]. Therefore, oxygen vacancies, double OH and single OH groups are all expected to be present in the initial period after sample preparation and should be considered in the identification of the defects in the AFM images. All types of species are, however, located *directly* on the oxygen sub-lattice (figure 1(d)), and we can thus directly deduce from our experimental AFM images that bright rows represent the Ti^{4+} sub-lattice in the AFM images in figure 2(a), while the O^{2-} rows are imaged as bright rows in the AFM images in figure 2(b), corresponding to the AFM tip apex being either negatively (figure 2(a)) or positively (figure 2(b)) terminated.

To determine the chemical identity of the defects we have thoroughly analysed a number of highly resolved AFM images with negative or positive tip termination, respectively. The images for this analysis were all recorded less than two hours after preparation in order to ensure an adequate population of vacancies relative to hydroxyls, and visual inspection of the defects in the AFM image obtained with a negative tip termination clearly shows that we can indeed discern three types of defect. Two types of very bright features are visible on the oxygen rows together with a much fainter feature bridging between the Ti rows. The three types of defect are shown in detail in figure 3(a), where each defect is represented by a zoom-in AFM image and a cross-section taken along the (dark) O rows (figure 3(b)). From the cross-sections, the defects are characterized in terms of the protrusion width (w) in the [001] direction of the rows and the height (h) relative to the dark O^{2-} sub-lattice, and the data are compiled into statistical histograms (figures 4(a) and (b)). The statistical analysis reveals a clear trimodal distribution for both parameters and it is concluded that the two brighter protrusions have an average height relative to the dark O rows of $h = 87 \pm 10$ and 105 ± 10 pm and a corresponding width of approximately $w = 0.97$ and 1.14 nm, respectively. The much fainter protrusion bridging between the Ti rows is imaged at $h = 35 \pm 10$ pm relative to the dark O rows and has an average extension of approximately $w = 0.81$ nm in the direction of the rows. For images recorded with the positive tip, we also see three types of defect. As illustrated in figure 3(c), one defect is imaged as a very faint depression in the oxygen rows, and two types of defect are imaged as very dark pits with a different width. From a statistical analysis of cross-sections, it is found that

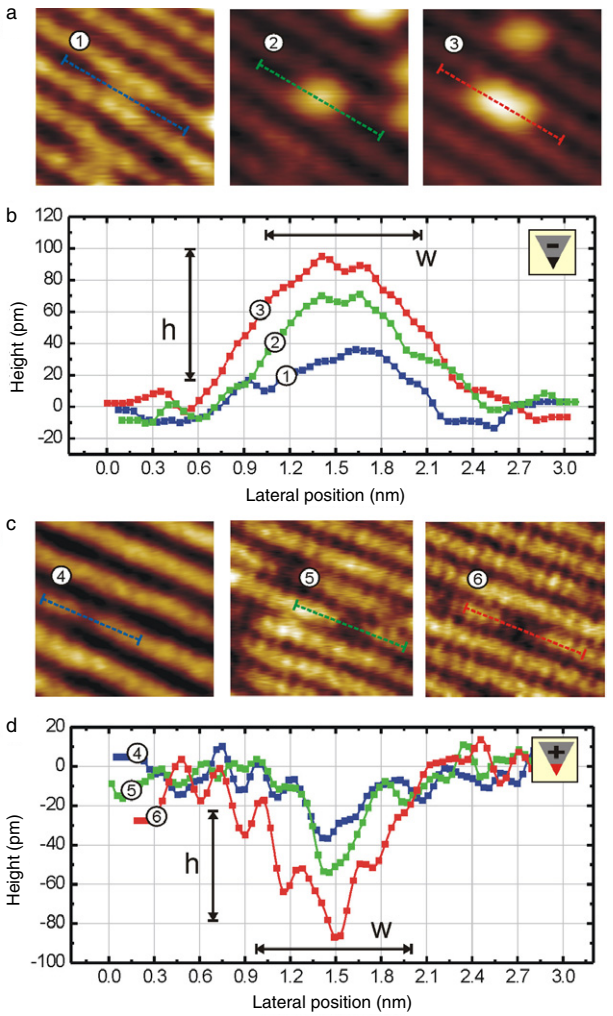

Figure 3. Series of 3 nm × 3 nm zoom-in images of the O vacancy and single OH or double OH groups on TiO_2 obtained with the same scanning parameters with a negative tip (a) or a positive tip (c), respectively. Note that the colour scale is independently optimized in the first images of (a) and (c), respectively, to better reveal the rather weak signature associated with the oxygen vacancy. (b) For the negative tip, cross-sections are taken in the [001] direction across the protrusions and measured relative to the dark O rows for the O vacancy (blue), single OH (green) and double OH (red). (d) Correspondingly for the positive tip, the cross-sections are taken across the three types of depressions and measured relative to the bright O rows. The width (w) is estimated based on the FWHM value of the peaks, and the height (h) is measured relative to the baseline of the O rows. Grid lines in the graphs represent the 0.3 nm interatomic distance of the two-fold coordinated atoms on the O rows.

the defects are imaged on average at $h = -25$ pm, -54 pm and -90 pm relative to the bright O^{2-} rows, respectively (uncertainty ± 10 pm). In the last two images of figure 3(c), the positions of atoms in the O^{2-} sub-lattice are resolved, and it is seen (figure 3(d)) that the widths of the defects closely adopt the ~0.3 nm interatomic distance between atoms in the O^{2-} rows, corresponding to either *one* or *two* lattice sites, respectively. In addition, the holes that occupy two lattice sites have a characteristic internal structure consisting of two protrusions separated by the regular interatomic spacing of the O^{2-} lattice and a -90 pm deep region located in the interstitial region between the two protrusions.

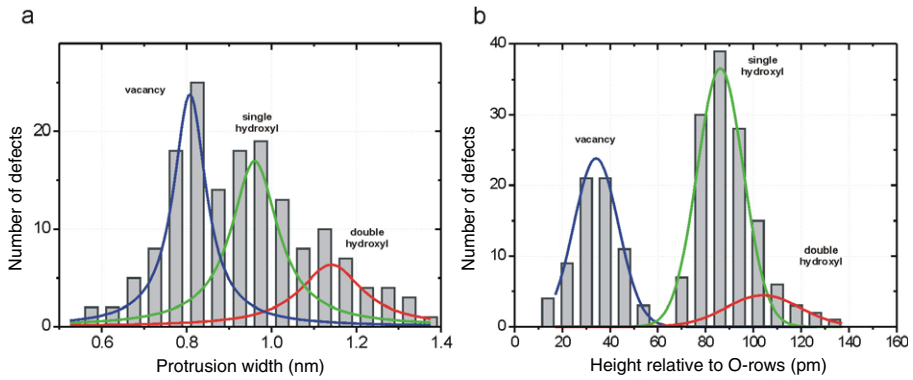

Figure 4. Statistical analysis of defects observed on $TiO_2(110)$ with a negatively terminated tip. The histograms are based on statistical material consisting of 28 consecutive low-drift images obtained with the same scanning parameters and without any sign of a tip change. $\Delta f = -14.4$ Hz and $V_{cp} = +1.54$ V. (a) Histogram of the width (w) of protrusions in the [001] direction measured in cross-sections. (b) Histogram of the protrusion height (h) relative to the dark O rows. The blue, red and green curves were obtained by peak fitting to outline the trimodal distribution of both histograms.

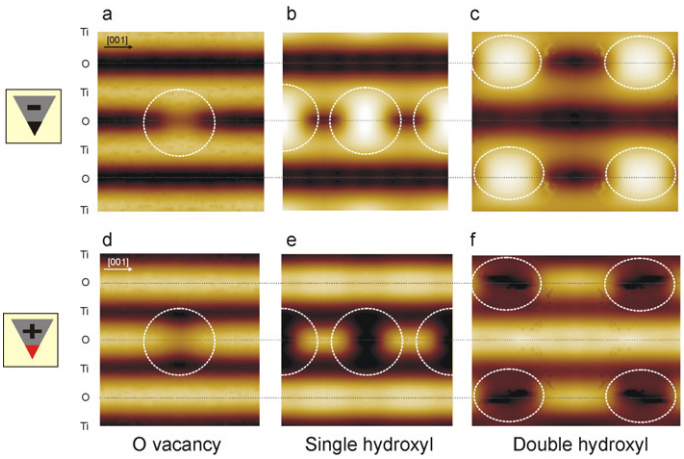

Figure 5. Simulated nc-AFM images of defects on the $TiO_2(110)$ surface. The first column shows images for the $TiO_2(110)$ surface with a single oxygen vacancy simulated with (a) a *negatively* terminated tip ($\Delta f = -14$ Hz) and (d) with a *positively* terminated tip ($\Delta f = -36$ Hz). Images (b) and (e) show simulated images of the $TiO_2(110)$ surface with single hydroxyls for both tip terminations (three OH in each image), and images (c) and (f) show the corresponding for double hydroxyls (i.e. two hydroxyls placed on neighbouring sites, four pairs are shown). Note that the asymmetry seen in the simulation at the double OH site is actually an artefact resulting from the asymmetric geometry of the double OH in the static simulation. Molecular dynamics simulations of the double OH configuration show that the motion of the hydrogen at room temperature will significantly smear out its appearance, producing a more symmetric contrast.

In figures 5(a)–(f) we present six simulated AFM images of the $TiO_2(110)$ surface with negative and positive tip termination, respectively, for TiO_2 surfaces with an isolated oxygen vacancy, isolated single OH groups and two OH groups placed on neighbouring sites. The simulations fully confirm our basic interpretation that imaging with a negatively terminated tip resolves the Ti^{4+} rows as bright and O^{2-} rows are imaged dark (figures 5(a)–(c)). Furthermore, a complete contrast reversal occurs when changing to a positive terminated tip (figures 5(d)–(f)). Note that for a negatively terminated tip, simulations reveal that rows of Ti^{4+} are imaged as bright, despite the fact that they are geometrically lower than the bridging oxygen atoms (see figure 1(d)). This is due to the attraction between the negative ion at the tip end and the positive five-fold coordinated Ti^{4+} ions in the surface. The interaction over the six-fold coordinated Ti^{4+} ions is actually found to be repulsive due to the proximity of negative bridging O^{2-}. In the simulations for the negatively terminated tip, both single (figure 5(b)) and double hydroxyl defects (figure 5(c)) appear as bright protrusions with a corrugation significantly higher than the bright Ti^{4+} rows. The single OH and double OH are easily discriminated by their respective heights of 86 pm and 112 pm with respect to the dark O row, in good agreement with the experimental values (see table 1). The vacancy in figure 5(a) is imaged as a protrusion of only 29 pm, lower than the bright Ti row (58 pm), and again

Table 1. Comparison of experimental and theoretical values.

	Negative terminated tip (−) Protrusion level relative to dark O rows (pm)		Positive terminated tip (+) Depression level relative to bright O rows (pm)	
Defect type	Experiment[a]	Theory	Experiment[a]	Theory
Vacancy	35	29	−25	−17
Single OH	89	86	−54	−64
Double OH	105	112	−90	−79

[a] The error was estimated to be ±10 pm for the experiment.

agreeing with experiment (35 ± 10 pm). Hence, we associate the first experimental image in figure 3(a) with an oxygen vacancy. The high corrugation of the OH groups relative to both O^{2-} and Ti^{4+} sub-lattices is ascribed to the stronger attractive interaction between the negative tip and the proton of the OH group. The contrast associated with the vacancy is, on the other hand, associated with the process of removal of a bridging oxygen and localization of the two remaining bonding electrons on nearby Ti atoms and within the vacancy itself [21, 22]. This renders the vacancy site less negative than the O^{2-} sub-lattice, and hence produces a brighter contrast at the site. The rather weak signature of the vacancy observed in the AFM images suggests that the charge localization is rather pronounced at the vacancy site. In extension of the present results, new studies combining site-specific force spectroscopy performed in the region surrounding the vacancy combined with simulations based on *ab initio* DFT could shed more light on the detailed charge distribution in the oxygen vacancy and may thus lead to a more complete theoretical description of the vacancy on $TiO_2(110)$.

For the positively terminated tip, the attraction between the positive apex and the negatively charged, protruding oxygen atoms produce a bright contrast on the bridging O^{2-} rows and the Ti^{4+} rows are images as dark in the simulation (figures 5(d)–(f)). Again, the oxygen vacancy is imaged as a rather faint signature, now appearing as a slight depression (-17 pm) on the bright oxygen rows in good agreement with the experimental corrugation of -25 ± 10 pm (table 1). Single and double OH groups are observed as dark pits on the bright row due to repulsion between the positive tip and the positive protons of the OH groups. In the simulation, the relative height of the single OH and double OH is -64 pm and -79 pm, again in good agreement with the experimental values of -54 ± 10 pm and -90 ± 10 pm, respectively (table 1). These findings are in sharp contrast to the simple picture that adsorbates physically sticking out of the surface should be imaged as bright with force microscopy. In summary, the simulations thus fully explain the observed contrast features, and we can discriminate in a qualitative and quantitative manner between oxygen vacancies, double hydroxyls and single hydroxyls observed experimentally on the TiO_2 surface.

The observation that the AFM tip can be functionalized *in situ* to discriminate between chemically different elements of an ionic surface may provide an attractive method to analyse other interesting metal oxide or ionic systems. In this study, preparing the tip in complementary charged modes allows us to understand the contrast pattern associated with defects and adsorbates on the surface, and hence unambiguously assign the observed features of the surface to the Ti and O atomic sub-lattices. The general electrostatic description of the tip–surface forces determined by the tip apex provides a relatively simple and clear interpretation of the contrast associated with the observed atom-resolved signatures. It should, however, be emphasized that the detailed appearance of the defects cannot easily be predicted from simple intuition, which is exemplified by the fact that a hydroxyl protruding physically from the surface is imaged as a hole much deeper than a real atomic vacancy. Indeed, holes on the TiO_2 surface observed in previous AFM studies were assigned to oxygen vacancies only, and the present studies call for a revision of these interpretations [6].

Acknowledgments

We wish to thank A L Shluger, R Schaub and S Wendt for enlightening discussions and M Sushko for help with the simulation parameters. JVL acknowledges financial support from the Danish Technical Research Council and the Carlsberg Foundation. ASF acknowledges support from the Academy of Finland.

References

[1] Zambelli T, Wintterlin J, Trost J and Ertl G 1996 *Science* **273** 1688
[2] Helveg S, Lauritsen J V, Lægsgaard E, Stensgaard I, Nørskov J K, Clausen B S, Topsøe H and Besenbacher F 2000 *Phys. Rev. Lett.* **84** 951
[3] Mitsui T, Rose M K, Fomin E, Ogletree D F and Salmeron M 2003 *Nature* **422** 705
[4] Binnig G, Quate C F and Gerber C 1986 *Phys. Rev. Lett.* **56** 930
[5] Giessibl F J 1995 *Science* **267** 68
[6] Fukui K, Onishi H and Iwasawa Y 1997 *Phys. Rev. Lett.* **79** 4202
[7] Orisaka S, Minobe T, Uchihashi T, Sugawara Y and Morita S 1999 *Appl. Surf. Sci.* **140** 243
[8] Barth C and Reichling M 2001 *Nature* **414** 54
[9] Barth C and Henry C R 2003 *Phys. Rev. Lett.* **91** 196102
[10] Bennewitz R, Foster A S, Kantorovich L N, Bammerlin M, Loppacher C, Schar S, Guggisberg M, Meyer E and Shluger A L 2000 *Phys. Rev.* B **62** 2074
[11] Tersoff J and Hamann D R 1983 *Phys. Rev. Lett.* **50** 1998
[12] Schaub R, Thostrup P, Lopez N, Lægsgaard E, Stensgaard I, Nørskov J K and Besenbacher F 2001 *Phys. Rev. Lett.* **87** 6104
[13] Wendt S *et al* 2005 *Surf. Sci.* **598** 226
[14] Bikondoa O, Pang C L, Ithnin R, Muryn C A, Onishi H and Thornton G 2006 *Nat. Mater.* **5** 189
[15] Yokoyama K, Ochi T, Sugawara Y and Morita S 1999 *Phys. Rev. Lett.* **83** 5023
[16] Sasaki N, Watanabe S and Tsukada M 2002 *Phys. Rev. Lett.* **88** 046106
[17] Gay D H and Rohl A L 1995 *J. Chem. Soc., Faraday Trans.* **91** 925
[18] Gale J D 1997 *J. Chem. Soc., Faraday Trans.* **93** 629
[19] Bandura A V and Kubicki J D 2003 *J. Phys. Chem.* B **107** 11072
[20] Grimes R W, Catlow C R A and Stoneham A M 1989 *J. Phys.: Condens. Matter* **1** 7367
[21] Bredow T and Pacchioni G 2002 *Chem. Phys. Lett.* **355** 417
[22] Rasmussen M D, Molina L M and Hammer B 2004 *J. Chem. Phys.* **120** 988
[23] Hofer W A, Foster A S and Shluger A L 2003 *Rev. Mod. Phys.* **75** 1287
[24] Foster A S, Pakarinen O H, Airaksinen J M, Gale J D and Nieminen R M 2003 *Phys. Rev.* B **68** 195410
[25] Foster A S, Gal A Y, Nieminen R M and Shluger A L 2005 *J. Phys. Chem.* B **109** 4554
[26] Bergstrom L 1997 *Adv. Colloid Interface Sci.* **70** 125
[27] García R and Pérez R 2002 *Surf. Sci. Rep.* **47** 197
[28] Giessibl F J 2003 *Rev. Mod. Phys.* **75** 949
[29] Barth C, Foster A S, Reichling M and Shluger A L 2001 *J. Phys.: Condens. Matter* **13** 2061
[30] Foster A S, Barth C, Shluger A L and Reichling M 2001 *Phys. Rev. Lett.* **86** 2373
[31] Diebold U 2003 *Surf. Sci. Rep.* **48** 53
[32] Kurtz R L, Stockbauer R, Madey T E, Román E and de Segovia J L 1989 *Surf. Sci.* **218** 178
[33] Hugenschmidt M B, Gamble L and Campbell C T 1994 *Surf. Sci.* **302** 329
[34] Linsebigler A, Lu G and Yates J T J 1995 *Chem. Rev.* **95** 735
[35] Suzuki S, Fukui K, Onishi H and Iwasawa Y 2000 *Phys. Rev. Lett.* **84** 2156